J Physiol 593.6 (2015) pp 1409–1427

The Journal of Physiology

Contribution of sodium channel neuronal isoform $Na_v1.1$ to late sodium current in ventricular myocytes from failing hearts

Sudhish Mishra[1], Vitaliy Reznikov[1], Victor A. Maltsev[2], Nidas A. Undrovinas[1], Hani N. Sabbah[1] and Albertas Undrovinas[1]

[1] *Department of Internal Medicine, Henry Ford Hospital, Detroit, MI, USA*
[2] *National Institute on Aging, Intramural Research Program, Baltimore, MD, USA*

Key points

- Late Na^+ current (I_{NaL}) contributes to action potential remodelling and Ca^{2+}/Na^+ changes in heart failure.
- The molecular identity of I_{NaL} remains unclear.
- The contributions of different Na^+ channel isoforms, apart from the cardiac isoform, remain unknown.
- We discovered and characterized a substantial contribution of neuronal isoform $Na_v1.1$ to I_{NaL}.
- This new component is physiologically relevant to the control of action potential shape and duration, as well as to cell Ca^{2+} dynamics, especially in heart failure.

Abstract Late Na^+ current (I_{NaL}) contributes to action potential (AP) duration and Ca^{2+} handling in cardiac cells. Augmented I_{NaL} was implicated in delayed repolarization and impaired Ca^{2+} handling in heart failure (HF). We tested if Na^+ channel (Na_v) neuronal isoforms contribute to I_{NaL} and Ca^{2+} cycling defects in HF in 17 dogs in which HF was achieved via sequential coronary artery embolizations. Six normal dogs served as control. Transient Na^+ current (I_{NaT}) and I_{NaL} in left ventricular cardiomyocytes (VCMs) were recorded by patch clamp while Ca^{2+} dynamics was monitored using Fluo-4. Virally delivered short interfering RNA (siRNA) ensured $Na_v1.1$ and $Na_v1.5$ post-transcriptional silencing. The expression of six Na_vs was observed in failing VCMs as follows: $Na_v1.5$ (57.3%) > $Na_v1.2$ (15.3%) > $Na_v1.1$ (11.6%) > $Na_v2.1$ (10.7%) > $Na_v1.3$ (4.6%) > $Na_v1.6$ (0.5%). Failing VCMs showed up-regulation of $Na_v1.1$ expression, but reduction of $Na_v1.6$ mRNA. A similar Na_v expression pattern was found in samples from human hearts with ischaemic HF. VCMs with silenced $Na_v1.5$ exhibited residual I_{NaT} and I_{NaL} (~30% of control) with rightwardly shifted steady-state activation and inactivation. These currents were tetrodotoxin sensitive but resistant to MTSEA, a specific $Na_v1.5$ blocker. The amplitude of the tetrodotoxin-sensitive I_{NaL} was 0.1709 ± 0.0299 pA pF^{-1} ($n = 7$ cells) and the decay time constant was $\tau = 790 \pm 76$ ms ($n = 5$). This I_{NaL} component was lacking in VCMs with a silenced $Na_v1.1$ gene, indicating that, among neuronal isoforms, $Na_v1.1$ provides the largest contribution to I_{NaL}. At –10 mV this contribution is ~60% of total I_{NaL}. Our further experimental and *in silico* examinations showed that this new $Na_v1.1$ I_{NaL} component contributes to Ca^{2+} accumulation in failing VCMs and modulates AP shape and duration. In conclusion, we have discovered an $Na_v1.1$-originated I_{NaL} component in dog heart ventricular cells. This component is physiologically relevant to controlling AP shape and duration, as well as to cell Ca^{2+} dynamics.

*A. Undrovinas is currently retired.

DOI: 10.1113/jphysiol.2014.278259

(Received 30 May 2014; accepted after revision 3 October 2014; first published online 3 October 2014)
Corresponding author A. Undrovinas: Henry Ford Hospital, Cardiovascular Research, Education and Research Bldg, Room 4015, 2799 West Grand Boulevard, Detroit, MI 48202-2689, USA. Email: adas7247@yahoo.com

Abbreviations AP, action potential; E–C, excitation–contraction; GFP, green fluorescent protein; HF, heart failure; I_{NaL}, late Na^+ current; I_{NaT}, transient Na^+ current; LV, left ventricular; MTSEA, 2-aminoethyl methanethiosulfonate hydrobromide; Na_v, sodium channel; siRNA, short interfering RNA; SSA, steady-state activation; SSI, steady-state inactivation; VCM, ventricular cardiomyocyte.

Introduction

A physiological role of neuronal isoforms of voltage-sensitive Na^+ channels (Na_vs) in heart has been suggested many years ago by Corabeouf (Coraboeuf *et al.* 1979) based on their result that low concentrations (33 nM) of tetrodotoxin (TTX) significantly shortened action potential (AP) duration recorded in cardiac Purkinje fibres. At this low concentration TTX blocks only so-called 'TTX-sensitive' Na_vs which are neuronal isoforms (Haufe *et al.* 2005*a*). Indeed, during the past decade, besides the dominating cardiac isoform main α-subunit, $Na_v1.5$, different transcripts of highly TTX-sensitive neuronal Na_v isoforms have been found in mouse ($Na_v1.1$, 1.3, 1.6) and dog ($Na_v1.1$, 1.2, 1.3) heart (Maier *et al.* 2004; Haufe *et al.* 2005*a*,*b*). These neuronal Na_vs are responsible for 10% and 20% of the peak transient Na^+ current, I_{NaT}, in dog myocardial and Purkinje cells, respectively (Haufe *et al.* 2005*b*). The contribution of neuronal Na_vs to the late Na^+ current, I_{NaL}, has not been studied in cardiac cells, therefore the molecular identity of I_{NaL} needs further careful consideration. This problem is especially important in HF where the gene expression profile changes dramatically. Thus an intriguing possibility could be that the differential expression of neuronal Na_vs can contribute, at least in part, to I_{NaL} alterations (augmentation) (Valdivia *et al.* 2005; Maltsev *et al.* 2007) and to I_{NaL}-related electrophysiological abnormalities observed in HF (for review see Maltsev & Undrovinas, 2008).

In the present study we used a combination of molecular and pharmacological approaches, as well as numerical modelling, to test a hypothesis that neuronal Na_v isoforms contribute to I_{NaL} in a physiologically significant manner in ventricular myocytes (VCMs) isolated from failing adult dog hearts. We performed post-transcriptional silencing of $Na_v1.1$ and $Na_v1.5$ genes by sequence-directed RNA using virally delivered short interfering RNA (siRNA). We found the expression of six Na_vs in both human heart and adult dog VCMs. Analysis of the expression revealed up-regulation of $Na_v1.1$ and down-regulation of $Na_v1.6$ in failing heart compared to normal heart. We took advantage of the method of culturing adult dog VCMs, established by our group, that preserves I_{NaT} and I_{NaL} over 5 days, i.e. sufficient time for gene silencing and membrane protein turnover (Maltsev *et al.* 2008*a*; Mishra *et al.* 2011). In VCMs with silenced $Na_v1.5$ we found a substantial residual I_{NaT} and I_{NaL}. Our biophysical and pharmacological examinations confirmed its neuronal isoform origin. Diastolic Ca^{2+} accumulation was reduced via blockade of the neuronal I_{NaL} component, indicating its physiological importance. Our numerical model simulations also demonstrated the physiological importance of the novel I_{NaL} component: the $Na_v1.1$- associated I_{NaL} effectively modulates AP shape and duration, as well as intracellular Ca^{2+} homeostasis.

Methods

HF model, human heart samples

The Henry Ford Health System Institutional Review Board approved all studies using human tissue and written informed consent was obtained. Studies conducted in animals as well as the methods of killing the animals were in accordance with the *Guidelines for the Care and Use of Laboratory Animals* (NIH publication No. 85-23), and were approved by the Henry Ford Health System Institutional Animal Care and Use Committee.

The dog model of chronic HF is similar by a vast array of functional and pathophysiological parameters (Sabbah *et al.* 1992) to that in humans. HF was produced in 17 dogs by multiple sequential coronary artery microsphere embolizations as previously described (Sabbah *et al.* 1991). All haemodynamic data were collected during cardiac catheterization performed under general anaesthesia and sterile conditions. Anaesthesia was induced using a combination of intravenous injections of hydromorphone (0.22 mg kg^{-1}) and diazepam (0.2–0.6 mg kg^{-1}), and maintained throughout the procedure with 1–2% isoflurane. All dogs were intubated and ventilated with room air supplemented with oxygen. At the end of data collection, and while the animal was still under general anaesthesia, the chest was opened via a left thoracotomy and the heart rapidly removed and tissue prepared for further studies. After each coronary microembolization session, dogs were weaned off of the respirator and allowed to recover. Animals were closely monitored until the endotracheal tube was removed and the dog was in a sternal position. Animals were then placed in post-operative recovery cages with incubated cloth blankets for warmth. Animals were given analgesics for

pain and/or medications for cardiovascular complications only if needed. The animals were monitored until pain medications and/or cardiovascular drugs were no longer needed. HF state was confirmed by haemodynamic and angiographic measurements. At the time of harvesting the hearts (~3 months after last embolization), left ventricular (LV) ejection fraction was 25 ± 1.2% ($n = 17$).

Human heart samples were obtained from explanted hearts from patients with chronic HF.

Cell culture and transfection

VCMs were enzymatically isolated from the apical LV mid-myocardial slices as previously reported (Maltsev *et al.* 1998*a*). The yield of viable rod-shaped, Ca^{2+}-tolerant VCMs varied from 40 to 70%. VCMs were cultured for 5 days (the time frame required for gene silencing; Maltsev *et al.* 2008*a*), as previously described (Maltsev *et al.* 2002). We added 10 μl of 5×10^8 virus particles ml^{-1} directly to the medium of the culture dish containing ~15×10^4 cells and cultured them further during the next 4 days (5 days total). Effectiveness of transfection was visually monitored in individual cardiomyocytes (Nikon Diaphot, 200) by green fluorescent protein (GFP) fluorescence (Fig. 3*A* inset) and by the occurrence of mRNA encoding GFP.

siRNA design

Double stranded hairpin siRNAs corresponding to the previously sequenced dog $Na_v1.5$ and $Na_v1.1$ (GenBank DQ665939 and AY126477, respectively) and other Na_vs were designed as recommended (Elbashir *et al.* 2001) and published by our group (Mishra *et al.* 2011). The details and sequences of silencing and non-silencing (control) siRNAs used in this study are given in Table 1. A BLAST search for these sequences against the GenBank database was performed and did not reveal matches with any other gene.

Real-time PCR and Western blot analysis

To quantify mRNA levels, we used both conventional gels and the fluorescence-based (SYBR green) kinetic real-time PCR performed using 7500 Fast Real-Time PCR Applied Biosystems (Life Technologies, Grand Island, NY, USA) sequence detection system. For each sodium channel isoform, several transcript-specific perfect match primer sets were designed and custom synthesized on the basis of sequences available in the NIH database. Primers were tested for production of predicted band size by RT-PCR. PCR products of correct band sizes were sequenced to check specificity. Each specific primer, which was selected after sequencing, was tested for use in real-time PCR before using in silencing experiments. Primers were also tested for amplification efficiency by standard curve analysis. Efficiencies of all the primers used in the study were between 90 and 99%. The quality of the amplified fragments was monitored using melting curve analysis and agarose gel electrophoresis. Quantitative values were obtained from the PCR quantification cycle number (Cq) at which point the increase in signal for the PCR product was exponential. The sets of primers are given in Table 2.

The relative mRNA abundance expressed as arbitrary units was calculated using expression levels of all transcripts normalized to glyceraldehyde 3-phosphate dehydrogenase (GAPDH) mRNA. This value was then normalized to mRNA levels measured from VCMs transfected with the non-silencing siRNA for the appropriate transcript ($2^{-\Delta\Delta Ct}$ method). Membrane protein preparations were obtained from approximately 3×10^6 myocytes as previously described (Zicha *et al.* 2004; Mishra *et al.* 2011). Antibody was detected with Western blot chemo-luminescence reagent (NEN Life Science Products, Boston, MA, USA). Western blots were considered specific if the peptide epitope reduced the band intensity. The resulting images of Western blots and PCR gels (See Fig. 2*A* and *B*) were scanned and the relative densities of bands were quantified using SigmaGel (Sigma-Aldrich, USA) or ImageJ (National Institute of Health free software) software. The primary polyclonal anti-$Na_v1.5$ and anti-$Na_v1.1$ antibodies were obtained from Alomone Labs (Jerusalem, Israel). Polyclonal calsequestrin antibody (Abcam Inc., Cambridge, MA, USA) was used for the protein loading control.

Electrophysiology

I_{Na} was recorded using conventional whole-cell patch-clamp techniques. Experimental and theoretical evaluation of the decay kinetics of I_{Na} and the steady-state activation (SSA) and inactivation (SSI) voltage dependency of I_{Na} were the same as we reported previously (Mishra *et al.* 2011). The decays of both I_{NaT} and I_{NaL} were approximated by double exponential fits, but the SSA and SSI were approximated by respective Boltzmann functions. Ca^{2+} signals were measured at 35 °C and 1.8 mM $[Ca^{2+}]_o$ using a photo-multiplier in field-stimulated single VCMs loaded with the acetoxymethyl ester form of Fluo-4, Fluo-4 AM (Undrovinas *et al.* 2010). I_{NaT} and I_{NaL} were measured at room temperature (21–23 °C).

Numerical excitation–contraction coupling model

To address the physiological significance of the neuronal I_{NaL} component, we used a modified excitation–contraction (E–C) coupling model of a failing canine ventricular myocyte developed previously by Winslow *et al.* (1999). The original model was modified

to include I_{NaL} equations as we previously reported (Undrovinas *et al.* 2010; Mishra *et al.* 2011). In this study we further modified I_{NaL} formulations to include two separate I_{NaL} components for cardiac and neuronal isoforms, respectively. Each component has its own activation and inactivation gating variables.

Statistical analysis

Statistics are reported as mean ± SEM with '*n*' representing the number of cells. Multiple comparisons between treatment groups were made using one-way analysis of variance (ANOVA) followed by Bonferroni's *post hoc* test. The significance of changes of theoretical SSA and SSI fits was evaluated with an *F* test (StatMost, Data-Most, Salt Lake City, UT, USA) for tabulated values predicted by the Boltzmann model at a confidence level of 0.95. Differences for both experimental data and model predictions were considered statistically significant for $P < 0.05$.

Results

Molecular biology data

We observed HF-related changes in mRNA levels of $Na_v1.1$ and $Na_v1.6$ in human and dog VCMs, whereas bands corresponding to $Na_v1.2$ were strong in both samples shown in Fig. 1*A* and *B*. The relative level of main α-subunit Na_v expression was compared by real-time PCR. We found transcripts of six genes encoding the Na^+ channel main α-subunit expressed in failing VCMs in the following order: $Na_v1.5$ (57.3%) > $Na_v1.2$ (15.3%) > $Na_v1.1$ (11.6%) > $Na_v2.1$ (10.7%) > $Na_v1.3$ (4.6%) > $Na_v1.6$ (0.5%). Statistical analysis in normal and failing hearts of both human and dog revealed up-regulation of $Na_v1.1$ expression, but reduction of $Na_v1.6$ mRNA levels (Fig. 1*C* and *D*) .

The adenovirus-delivered $Na_v1.5$-siRNA reduced (in time-dependent fashion) the numbers of transcripts of the main α-subunit of the cardiac Na^+ channel isoform (Fig. 2*A*), as well as its protein level (Fig. 2*B*). This inhibition of gene expression is specific to $Na_v1.5$, without a cross-reaction with the genes expressing auxiliary β-subunits (not shown) or other Na_vs (Fig. 2*C*).

Patch-clamp data

Patch-clamp data experiments were performed in HF dog VCMs infected with adenovirus-$Na_v1.5$-siRNA. Our previous studies with specific oligonucleotides (Maltsev *et al.* 2008*a*) have shown that $Na_v1.5$ provides a dominant contribution to I_{NaL}. Indeed, silencing of the $Na_v1.5$ gene in the present study also resulted in a significant and substantial reduction (by about 70%) of the peak transient Na^+ current, I_{NaT}, shown in Fig. 3. Furthermore, the results of our patch clamp experiments in Fig. 3*B* and *C* show that there was a prominent and statistically significant rightward shift of the SSA ($V_{1/2G} = -40.9 \pm 1.7$ mV, $K_G = 6.5$ mV, $n = 8$ in control *vs.* 36.8 ± 1.6 mV, $K_G = 6.9$ mV, $n = 5$ in $Na_v1.5$-siRNA, $P < 0.05$ when $V_{1/2\,G}$ was compared) and SSI ($V_{1/2A} = 81.3 \pm 1.8$ mV, $K_A = -6.6$ mV, $n = 8$ in control *vs.* $V_{1/2A} = 70.3 \pm 2.3$ mV, $K_A = -6.4$ mV, $n = 5$, $P < 0.05$ when $V_{1/2A}$ was compared). G and A stands for activation and inactivation, respectively. These results illustrate that the remaining pool (whole or part) of Na^+ channels demonstrates activation and inactivation characteristics different from that for $Na_v1.5$. It is known that the neuronal Na^+ channels activate at more depolarized potentials (Haufe *et al.* 2005*b*). Therefore these results support the idea that neuronal channels may contribute to the remaining I_{NaT} in these failing VCMs.

To further explore the idea of the neuronal isoforms' contribution to I_{NaT}, we used 2-aminoethyl methanethiosulfonate hydrobromide (MTSEA), which is known to block only cardiac and not neuronal isoforms of the Na^+ channel (Haufe *et al.* 2005*b*). In the freshly isolated failing VCMs we found a substantial portion of I_{NaT} (~20%) that was MTSEA resistant (Fig. 4). While this component was smaller than the remaining I_{NaT} after $Na_v1.5$ post-transcriptional silencing (~30%) (Fig. 4*C*), it can still be physiologically significant (as we show below).

Table 1. DNA sequences for coding siRNA designed to silence different genes that encode the Na^+ channel isoform main α- and auxiliary β-subunit used in this study to make the adenovirus

$Na_v1.1$-A3906F	5′-GATCATCTCTCAGGACACTAAGAGCGGAATTCGGCTCTTAGTGTCCTGAGAGATTTTTT-3′
$Na_v1.2$A-1683F	5′-GATCCCGTAAATTGGTTCCTATCGTCTGTTGAATTCCGCAGACGATAGGAACCAATTTATTTTTTCCAAA-3′
$Na_v1.3$-B5191F	5′-GATCCGTCAGAGCAAAGAGCAGTGTGCTTGAATTCCGGCACACTGCTCTTTGCTCTGATTTTTTCCAA-3′
$Na_v1.5$–190F	5′-GATCAAAGCTGCCAGATCTCTATGGGATCGATGCCATAGAGATCTGGCAGCTTTTTTTT-3′
$Na_v1.6$-A1271F	5′-GATCCGTGAGTCGGTCTAACATCTGCTTTGAATTCCGAGCAGATGTTAGACCGACTCATTTTTTCCAA-3′
$Na_v2.1$-A88F	5′-GATCGAGTGTGGATCTTCTGGAGAAGGAATTCGTTCTCCAGAAGATCCACACTCTTTTT-3′
NEG-CTRL-F	5′-GATCCCGTCGCTTACCGATTCAGAATGGTTGATATCCGCCATTCTGAATCGGTAAGCGATTTTTTCGA-3′
$Na_v\beta1$–202F	5′-GATCGAAGATCCACATTGAGGTGGTGATCGATGACCACCTCAATGTGGATCTTCTTTTT-3′
$Na_v\beta2$–216F	5′-GATCCAACTGCTCTGAGGAGATGTTGATCGATGAACATCTCCTCAGAGCAGTTGTTTTT-3′

In the next series of experiments we tested if these channels with different SSA and SSI characteristics contribute to I_{NaL}. To unmask the contribution of neuronal Na_vs to I_{NaL} we deliberately silenced $Na_v1.5$ gene expression by the virally delivered $Na_v1.5$-siRNA in these cells. $Na_v1.5$-siRNA caused a substantial I_{NaL} reduction with an apparent slower decay of the remaining I_{NaL} (Fig. 5*A*). The density of I_{NaL} evaluated at –30 mV significantly decreased in cells infected with the virus containing $Na_v1.5$-siRNA compared to freshly isolated

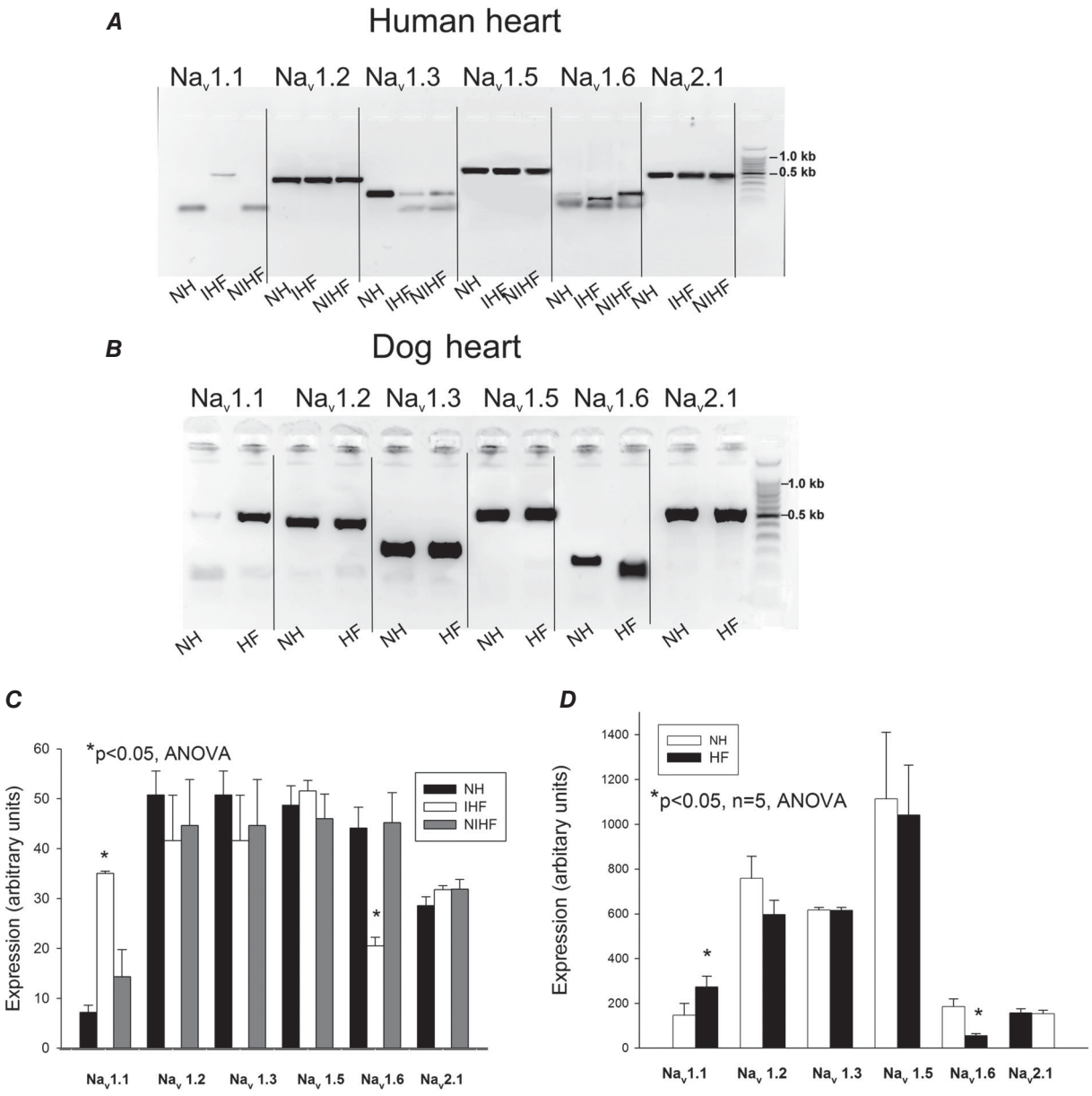

Figure 1. Expression of genes encoding different Na^+ channel isoforms Na_vx
RT-PCR analysis of Na_v transcripts in normal and failing human (*A*) and dog (*B*) left ventricular tissue samples. *A*, from left to right: $Na_v1.1$ isoform obtained in normal heart (NH), in explanted heart from patients with ischaemic (IHF), and non-ischaemic (NIHF) heart failure, respectively. The expected 491 bp band was not detected in NH and NIHF, $Na_v1.2$ isoform (417 bp), $Na_v1.3$ isoform (189 bp), $Na_v1.6$ isoform. A specific band of 155 bp is missing in IHF; a non-specific smaller band is present instead. $Na_v2.1$ isoform (586 bp). *B*, the same Na^+ channel isoforms as shown in *A* were obtained in dog normal (NH) and failing (HF) hearts. Last gel lane on right represents standard bp marker. *C*, summary data with statistics for Na_v isoforms expressed in human heart. RT-PCR gels were analysed in 5–7 tissue samples from left ventricles, *D*, summary data with statistics for Na_v isoforms expressed in dog heart. RT-PCR gels were analysed in 5 samples of ventricular cardiac myocytes from left ventricles of normal dog hearts and failing dog hearts, respectively. $^*P < 0.05$, ANOVA, data are mean ± SEM for both *C* and *D*.

cells and to cells infected with the non-silencing siRNA expressing GFP (Fig. 5*B*). Analysis of SSA and SSI in these cells clearly shows a rightward shift of the $V_{1/2}$ (Fig. 5*C* and *D*) as we found for I_{NaT}. We then fitted this I_{NaL} component to a two exponential decay function (yielding 'slow' and 'fast' sub-components, respectively). The slow sub-component of I_{NaL} decay (probably corresponding to the late scattered mode; Maltsev & Undrovinas, 2006) of the remaining I_{NaL} was significantly slower (Fig. 5*F*). The first (i.e. fast) exponent that corresponds to the burst mode (Maltsev & Undrovinas, 2006) remained unchanged (not shown). Therefore these data reveal a different Na_v contribution to I_{NaL} in failing VCMs.

To further study the neuronal isoform-generated I_{NaL} component, we used low concentrations (100 nM) of TTX in VCMs with silenced $Na_v1.5$ expression (results of these experiments are shown in Fig. 6*A* and *B*). Under these conditions the contribution of the cardiac (TTX-resistant)

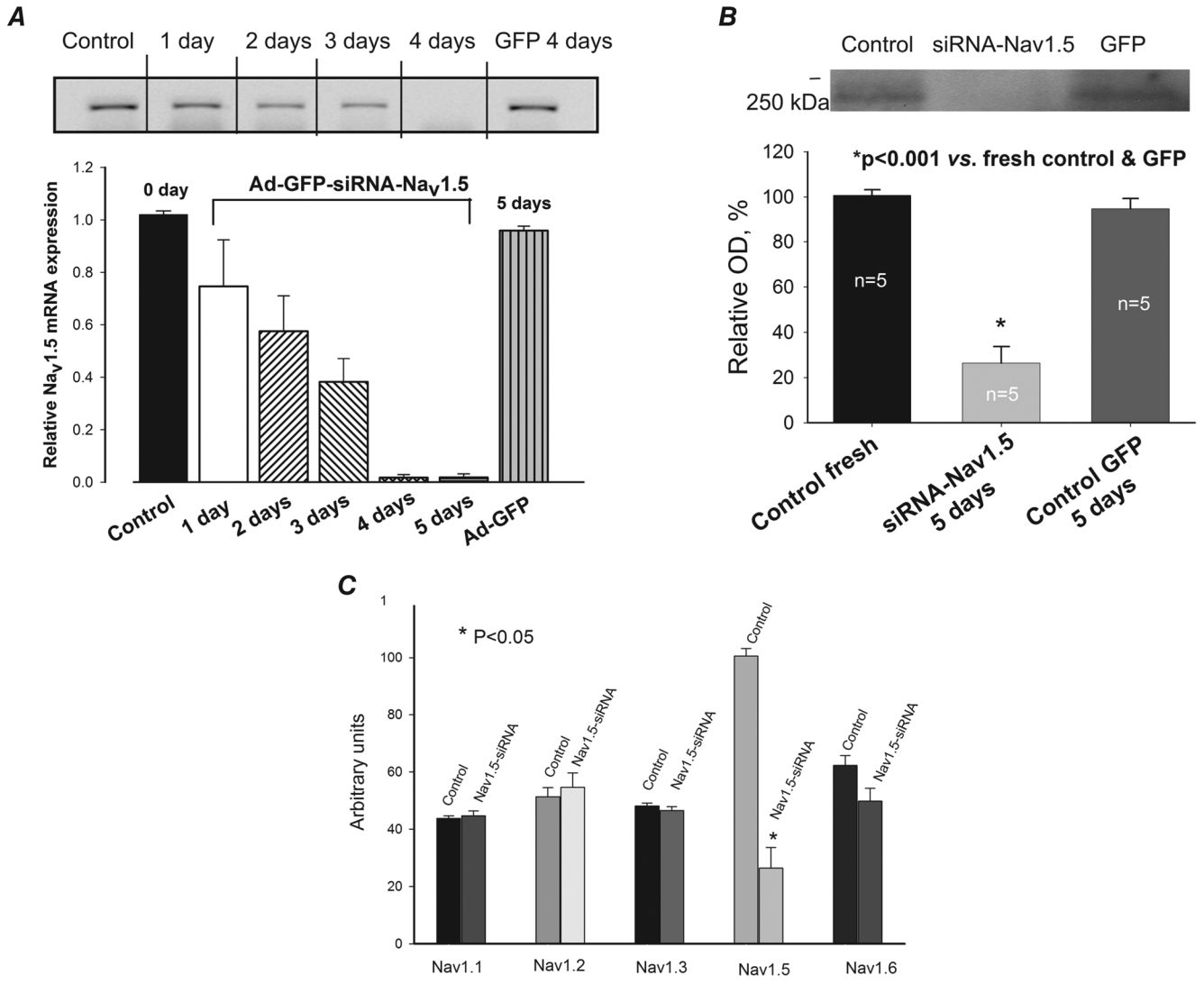

Figure 2. Silencing of *SCN5A* gene that encodes $Na_v1.5$ in LV cardiomyocytes of dog with chronic HF by virally delivered siRNA

A, RT-PCR analysis of mRNA abundance in control (fresh isolated cells), in cells infected with virus that contains cDNA for $Na_v1.5$ siRNA + GFP (Ad-GFP-$Na_v1.5$) and GFP alone (Ad-GFP). Upper panel: representative gel of such analysis performed at different times after the virus infection. Lower panel: summary data with statistical analysis of experiments similar to that shown in the upper panel obtained in 5–7 cells. Relative $Na_v1.5$ mRNA is given as relative to control density of bands. $^*P < 0.05$, *vs.* control and GFP. *B*, Western blot analysis of $Na_v1.5$ protein abundance in control, and in Ad-GFP-$Na_v1.5$- and Ad-GFP-treated cells. $^*P < 0.001$, *vs.* control and Ad-GFP. *C*, RT-PCR analysis of different sodium channel isoforms after transfection with $Na_v1.5$-siRNA (from 4 to 8 samples). $^*P < 0.05$. Statistically significant changes in *A*, *B* and *C*, were evaluated by the ANOVA test followed by Bonferroni's *post hoc* test. Data are mean ± SEM.

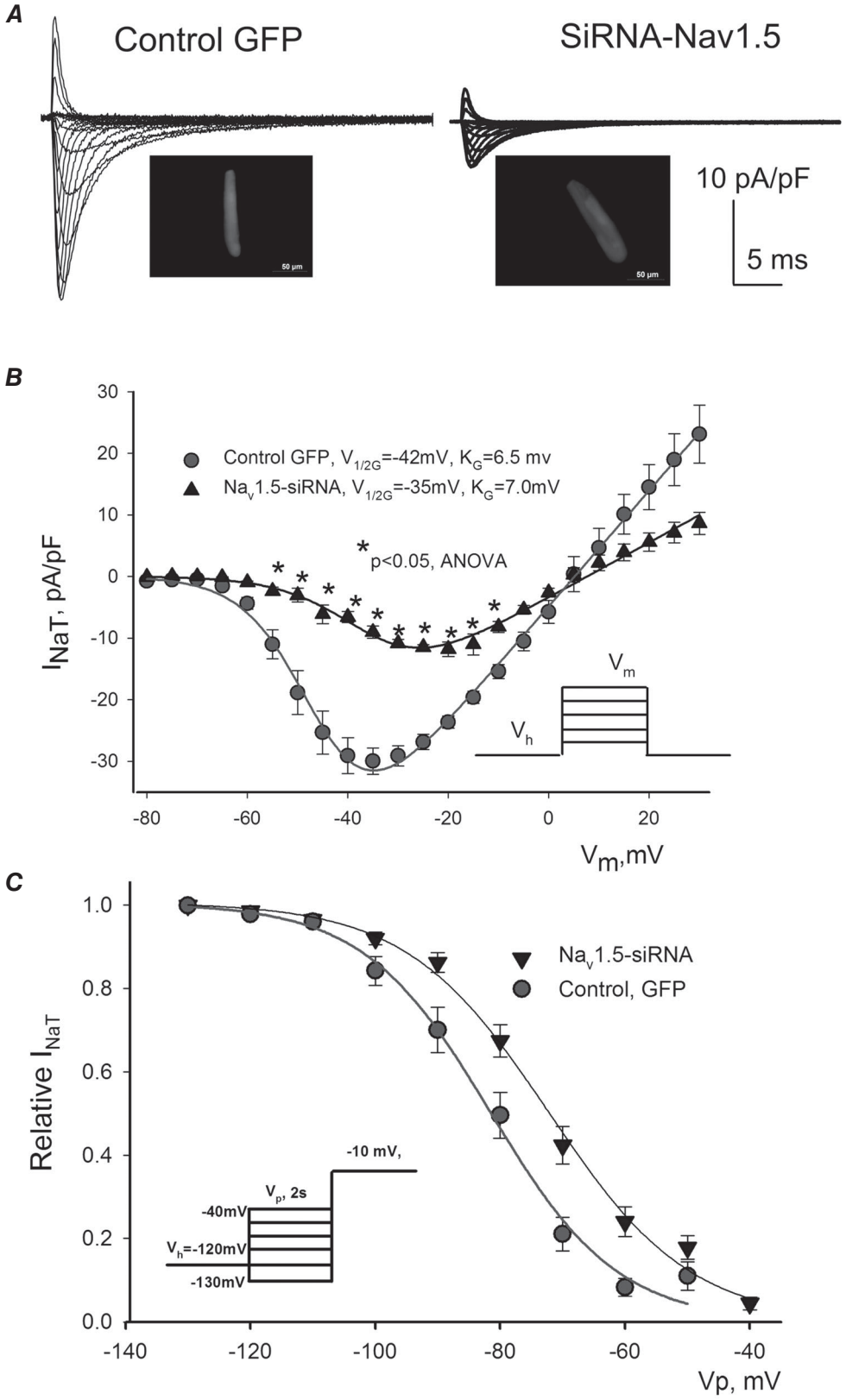

Figure 3. Post-transcriptional *SCN5A* gene silencing results in functional reduction of the transient Na^+ current, I_{NaT}, and reveals non-cardiac Na^+ channel component in LV cardiomyocytes from dog with chronic heart failure

Table 2. Sequences of primers used in this study for the real-time PCR

Isoform	Sequences	Product size (bp)
$Na_v1.1A$	F 5′-CCTGGTGTTCATTGTGTTGTTC	491
	R 5′-AATCGGGTGGTTTACTGTTGAG	
$Na_v1.2A$	F 5′-TCAAGAGAGTTCAGTGGTGCTG	418
	R 5′-AGTCTCTCCGGCTGTCATTGT	
$Na_v1.3A$	F 5′-CTACCACATCTCCTCCTTCCT	189
	R 5′-TCCAGTTGACACATAGACTTTACCA	
$Na_v1.5A$	F 5′-CCCAGAAGCAGGATGAGAAG	516
	R 5′-CGGTGAAGGTGTACTCGACA	
$Na_v1.6A$	F 5′-CAGCAGATGTTAGACCGACTCA	155
	R 5′-CTCCTTGGCACTCTTTGAGC	
$Na_v2.1A$	F 5′-TATTTGCTGGTTGGGATGG	586
	R 5′-ACTGCCTCTTGTTTTCGTTTCA	
$Na_v\beta1$	F 5′-TATGAGAATGAGGTGTTGCAGCTGG-3′	482
	R 5′-ATACGGCTGGCTCTTCCTTGAGG-3′	
$Na_v\beta2$	F 5′-CCGACTAACATCTCAGTCTC-3′	211
	R 5′-CTGTTTGTGGTTCACTGTG-3′	

Na^+ channel must remain almost unchanged. However, application of TTX to these myocytes caused a marked reduction of I_{NaL} (Fig. 6*A*). We then evaluated the revealed TTX-sensitive current as the difference between the recordings before and after TTX application (Fig. 6*B*). This TTX-sensitive current, presumably carried by the neuronal Na_vs, was slowly inactivating in a single-exponential manner. The amplitude of the TTX-sensitive I_{NaL} was 0.1709 ± 0.0299 pA pF^{-1} (n = 7 cells) and the decay time constant was $\tau = 790 \pm 76$ ms ($n = 5$ cells) recorded at $V_m = -10$ mV. These values we used in our numerical model simulations to evaluate the physiological significance of the neuronal I_{NaL} component (see below). The experimental current-to-voltage relation (*I–V* curve) for such experiments and theoretical (Boltzmann function) fits are shown in Fig. 6*C*. The *I–V* for the TTX-sensitive current was calculated (squares) as a subtraction of two *I–V* curves (circles and triangles). It is clearly seen that the difference *I–V* is shifted rightwards and we found the average SSA parameters for this component to be as follows: $V_{1/2G} = -24.1 \pm 1.0$ mV, and slope $K_G = 5.7 \pm 0.3$ mV *vs.* control $V_{1/2G} = -38.5 \pm 1.2$ mV, $K_G = 5.6 \pm 0.9$ mV. The *I–V* relationship analysis revealed a significant neuronal I_{NaL} component within the range of the AP plateau (Fig. 6*C*). These parameters of TTX-sensitive I_{NaL} were also used in our numerical modelling .

To further study the molecular identity of the TTX-sensitive I_{NaL}, we made adenovirus-based constructs containing cDNA templates for endogenous transcription of the GFP reporter gene, and cognitive siRNA, targeting different Na_v isoforms that are expressed in human and dog LV cardiomyocytes according to our data (Fig. 1). As shown in Fig. 7, transfection of failing dog VCMs with adenovirus containing $Na_v1.1$-siRNA significantly reduced both mRNA abundance (Fig. 7*A*) and $Na_v1.1$ protein level (Fig. 7*B*) without cross-reacting with other Na^+ channel isoforms (Fig. 7*C*). Furthermore, we found that application of MTSEA completely blocked I_{NaL} in failing VCMs (shown in Fig. 8*A* and *B*) with silenced $Na_v1.1$. At the same time, application of 100 nM TTX was not effective in VCMs with the silenced expression of $Na_v1.1$ (Fig. 8C). Figure 8*D* shows evaluated I_{NaL} densities measured at –10 mV in GFP control (0.3387 ± 0.06 pA pF^{-1}), $Na_v1.5$-siRNA (0.2123 ± 0.023 pA pF^{-1}) and $Na_v1.1$-siRNA (0.1737 ± 0.018 pA pF^{-1}). Therefore at this membrane potential the $Na_v1.1$-originated I_{NaL} component (~60% of total I_{NaL}) is comparable with $Na_v1.5$-originated I_{NaL} (i.e. remaining ~40% of total I_{NaL}). Furthermore, in our *in silico* simulations of APs we compared the dynamic contributions of these components and confirmed that $Na_v1.1$ provides a major contribution to total I_{NaL} during the AP plateau (see below). Based on these data, further studies with other Na_vs contributions to I_{NaL} seemed to be irrelevant and results are not shown. These data support the idea that $Na_v1.1$ is the major Na^+ channel isoform underlying the TTX-sensitive component of I_{NaL} in failing VCMs.

A, representative raw traces of I_{NaT} were recorded at different membrane potentials (V_m) in cells 5 days after infection with virus containing control non-silencing siRNA and cDNA for GFP (control GFP, left), and siRNA-$Na_v1.5$ (right). Cell images expressing GFP are shown in insets. *B*, average data from peak I_{NaT}–voltage relationship obtained in cultured cells for 5 days with virally delivered control siRNA (● control GFP, $n = 6$), and $Na_v1.5$-siRNA (▲, $n = 7$). We found a statistically significant reduction of I_{NaT} in response to $Na_v1.5$-siRNA in a wide range of potentials (*). Continuous lines show theoretical curves fitted to experimental current–voltage (*I–V*) data points to evaluate the steady-state activation (SSA) parameters which are given in the panel.●, control GFP, control siRNA ($n = 18$);▲, $Na_v1.5$-siRNA ($n = 16$). *C*, average experimental data of steady-state inactivation (SSI) data points in control (●, $n = 17$) and after *SCN5A* gene silencing by the siRNA (▲, $n = 16$) along with the fit to a Boltzmann function. The *F* test revealed a statistically significant ($P < 0.05$) difference between theoretical fits (*B* and *C*), and statistical significance, $P < 0.05$, between experimental data points presented as mean ± SEM (*B*) was evaluated by ANOVA followed by Bonferroni's *post hoc* test. Voltage clamp protocols are shown in *B* and *C* insets; V_h, holding and V_p, pre-pulse potentials, respectively.

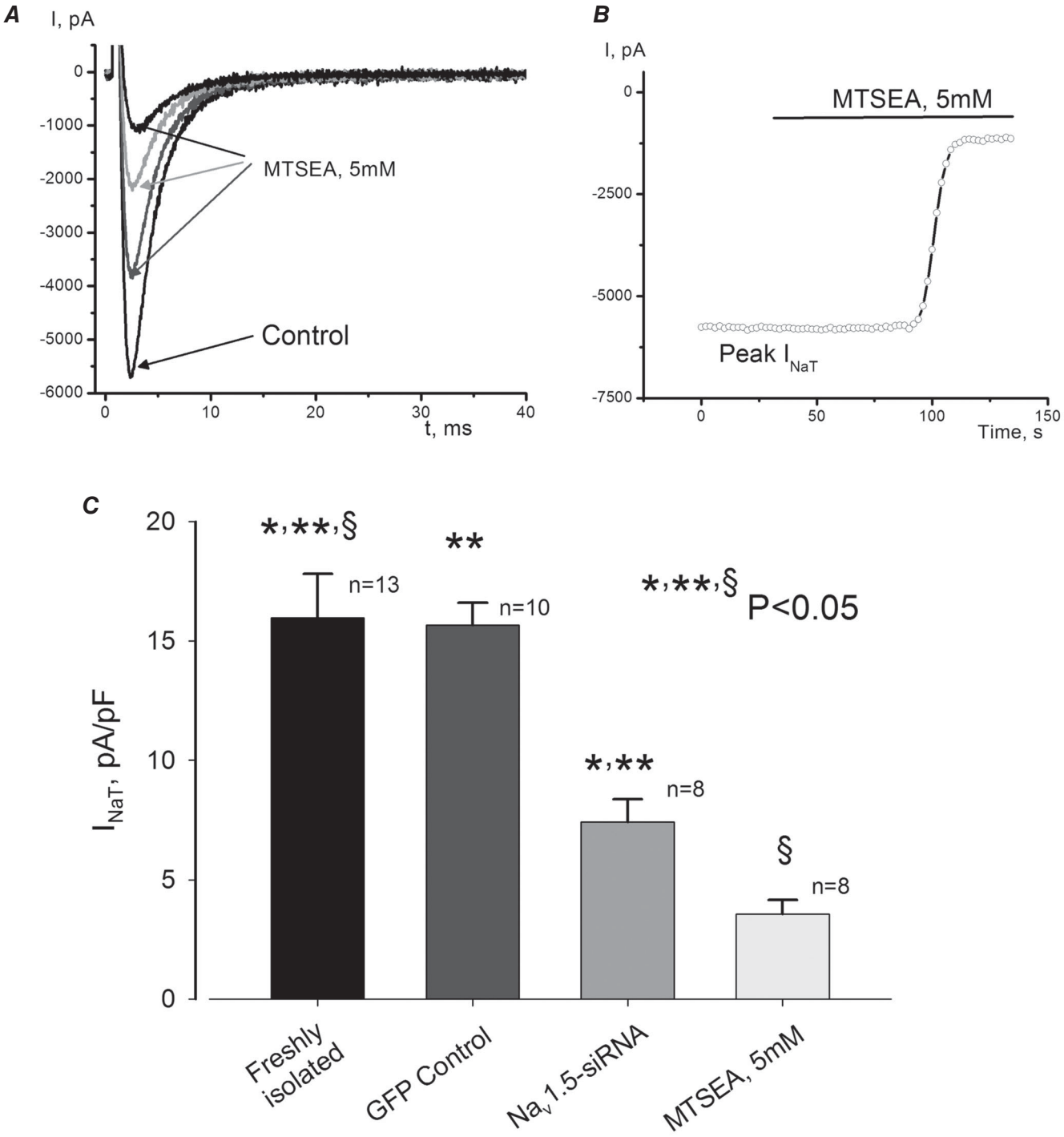

Figure 4. Contribution of non-cardiac Na^+ channel isoforms to I_{NaT} in LV cardiomyocytes of dogs with HF

A, consecutive raw I_{NaT} traces recorded before (control) and during MTSEA application in freshly isolated cells. *B*, time course of MTSEA effect on the peak I_{NaT} recorded in the same cell as shown in *A*. *C*, summary data and statistical analysis of I_{NaT} density in freshly isolated control and MTSEA-treated cells and infected cells with virus containing non-silencing siRNA or $Na_v1.5$-siRNA. Statistically significant changes, $P < 0.05$, were found in both groups evaluated by the ANOVA test followed by Bonferroni's *post hoc* test (*,** $Na_v1.5$-siRNA vs. freshly isolated control and GFP control, respectively, § MTSEA vs. freshly isolated control) I_{NaT} was recorded at –10 mV. Data are mean ± SEM.

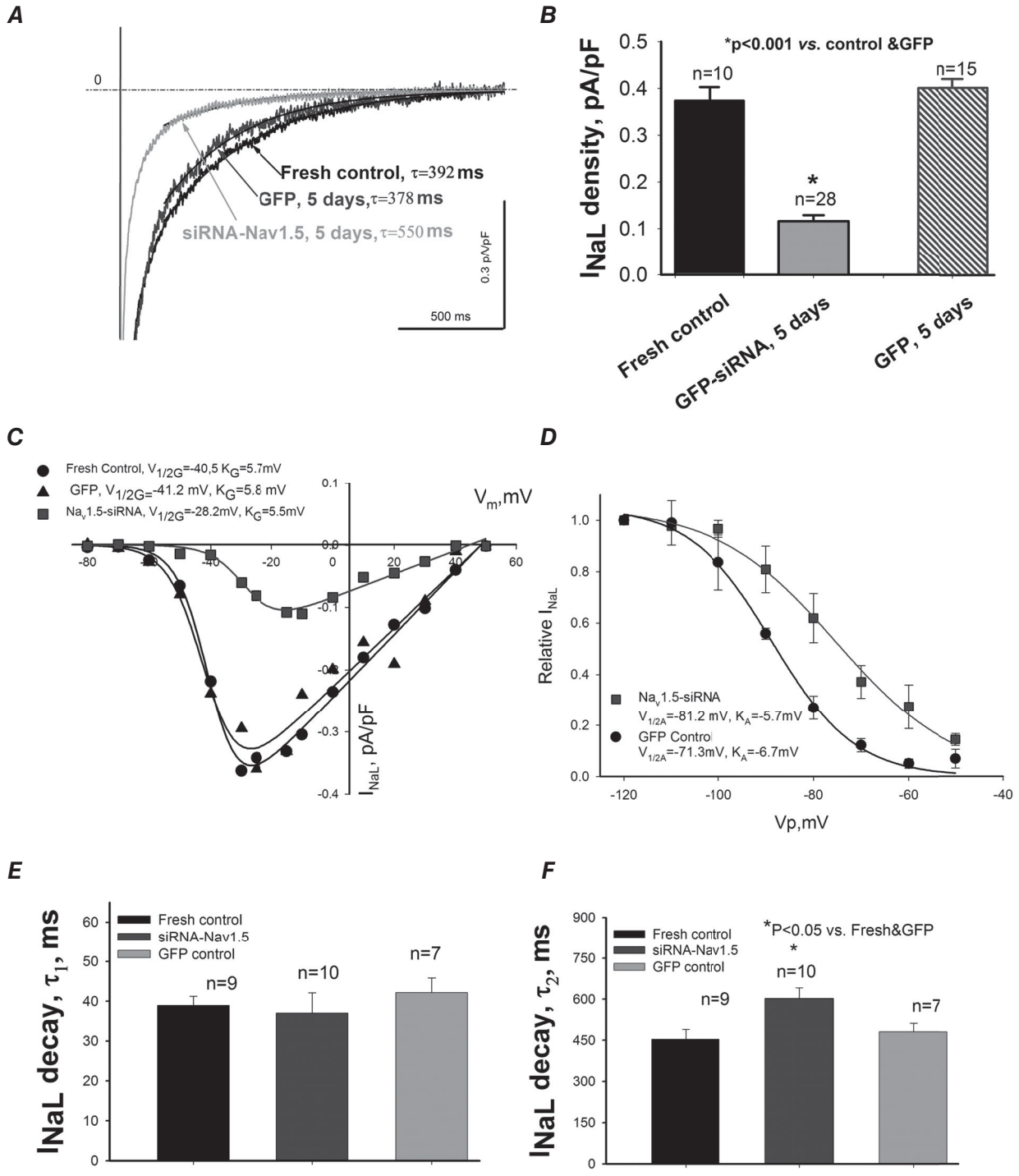

Figure 5. Post-transcriptional *SCN5A* gene silencing results in functional reduction of the late Na^+ current, I_{NaL}, and unmasks non-cardiac Na^+ channel component in LV cardiomyocytes from dog with chronic heart failure

A, representative raw traces of I_{NaL} were recorded at membrane potentials $V_m = -10$ mV in freshly isolated cells, and in cells 5 days after infection with virus containing control non-silencing siRNA and cDNA for GFP and siRNA-$Na_v1.5$ (indicated by the arrows). Exponential fits to I_{NaL} decay are shown by continuous lines and are superimposed with traces. Values of slow exponent time constant, τ, are given in the panel. *B*, summary data with statistics for I_{NaL} density. *C*, representative I_{NaL}–voltage relationship obtained in freshly isolated (●) and cultured cells for 5 days with virally delivered control siRNA (▲ control GFP), and $Na_v1.5$-siRNA (■). Continuous lines show theoretical curves fitted to experimental current–voltage (*I–V*) data points to evaluate steady-state activation (SSA)

Intracellular Ca^{2+} dynamics data

In the next series of experiments we addressed the question of the physiological importance of the neuronal I_{NaL} component in failing heart. Indeed, we found that blockade of neuronal I_{NaL} by low concentrations of TTX reduced diastolic Ca^{2+} accumulation in response to a 1.5 Hz pulse train in freshly isolated failing VCMs (Fig. 9).

Numerical model simulations of the neuronal component of I_{NaL}

To further address the physiological significance of the neuronal I_{NaL} component, we used a modified E–C coupling model in which we carefully introduced experimentally obtained I_{NaL} density, decay kinetics, as well as SSA and SSI parameters. The model predicted I_{NaL} traces and *I–V* relationship in good agreement with those obtained in our voltage-clamp experiments (compare Figs 5, 6 and 8 with Fig. 10*A*). We tested the physiological importance of the novel neuronal type I_{NaL} by numerical simulations of I_{NaL} dynamics during APs (Fig. 10*B*). Our simulations showed that the neuronal I_{NaL} lasts during the whole AP plateau and its amplitude (especially at the late phase of the plateau where it amounted to 60% of cardiac I_{NaL}), indicating that the neuronal component of I_{NaL} is a major player in the ion current balance during the AP plateau. Indeed, this new I_{NaL} neuronal component can significantly modulate (prolong) AP. In concert with the cardiac I_{NaL}, neuronal I_{NaL} leads to AP prolongation and to a higher and longer plateau of the AP (Fig. 10*C*), i.e. reproducing well-known features of failing myocardium. Next we numerically evaluated cytosolic Ca^{2+} dynamics during a 1.5 Hz pulse train. Introduction of the neuronal I_{NaL} component significantly increased diastolic Ca^{2+} accumulation at the end of the pulse train (Fig. 10*D*), which is in a good agreement with the experimental data (Fig. 9).

Discussion

Using a combination of post-transcriptional gene silencing by siRNA interference with the pharmacological approaches, cell electrophysiology (patch-clamping), intracellular Ca^{2+} monitoring, and numerical modelling, we discovered and characterized a novel neuronal component of I_{NaL} in dog ventricular cardiomyocytes. We also found that expression of the $Na_v1.1$ gene is responsible for the molecular identity of the neuronal I_{NaL} component. This component seems to be involved in E–C coupling by affecting AP shape and duration as well as intracellular Ca^{2+} dynamics. Furthermore, as discussed below in detail, the neuronal I_{NaL} component may provide a novel cellular and molecular mechanism contributing to major abnormalities associated with chronic HF, such as the impaired, rate-dependent (Rao *et al.* 2007; Logeart *et al.* 2009; Undrovinas *et al.* 2010) diastolic function and repolarization (for review see Maltsev & Undrovinas, 2008).

After I_{NaL} had been discovered in human hearts (Maltsev *et al.* 1998*a*) it was implicated in HF-related rhythm and contractility deficiencies (for review see Maltsev & Undrovinas, 2008). The importance of the augmented I_{NaL} contribution to HF mechanisms has been demonstrated in a series of experiments in which 'correction' of I_{NaL} in failing cardiomyocytes resulted in: (1) rescue of normal repolarization, (2) improvement (decreasing) of repolarization beat-to-beat APD variability, and (3) improvement of Ca^{2+} handling and contractility (Maltsev *et al.* 1998*b*; Undrovinas *et al.* 1999, 2006; Maltsev *et al.* 2007). Accordingly I_{NaL} has emerged as a novel possible target for cardioprotection to treat the failing heart (Maltsev *et al.* 2001, 2007; Noble & Noble, 2006; Maltsev & Undrovinas, 2008; Undrovinas & Undrovinas & Maltsev, 2008).

Therefore, the study of modulatory factors and the molecular identity of I_{NaL} is of obvious importance from both therapeutic and scientific standpoints. Modulatory mechanisms leading to I_{NaL} augmentation and decay slowing include: (1) the effects of the Na^+ channel protein microenvironment, such as sub-sarcolemmal cytoskeleton (Undrovinas *et al.* 1995; Maltsev & Undrovinas, 1997), lipid bilayer composition (Undrovinas *et al.* 1992) and auxiliary β-subunits (Mishra *et al.* 2011); and (2) the Ca^{2+}/calmodulin/calmodulin kinase signalling pathway (Maltsev *et al.* 2008*a*). Recent discoveries of the expression of array of different Na^+ channel isoforms in hearts indicate a possibility for new molecular mechanisms for I_{NaL} modulation, i.e. the different Na^+ channel isoform contributions to I_{NaL} that were the main objective of the present study.

Molecular identity

We found transcripts of six genes encoding the Na^+ channel main α-subunit expressed in both human

parameters which are given in the panel. *D*, average experimental data of steady-state inactivation (SSI) data points in control (●, $n = 17$) and after *SCN5A* gene silencing by the siRNA (■, $n = 16$) along with the fit to a Boltzmann function. *E* and *F*, statistical data for I_{NaL} decay time course evaluated by the double exponent fit. Difference between theoretical fits (*C* and *D*) was statistically significant ($P < 0.05$) evaluated by *F* test. Statistical significance, $P < 0.05$, between experimental data points presented as mean ± SEM (*B*, *E* and *F*) were evaluated by ANOVA followed by Bonferroni's *post hoc* test.

and dog failing hearts and the abundance of mRNA was in the following order: $Na_v1.5$ (57.3%) > $Na_v1.2$ (15.3%) > $Na_v1.1$ (11.6%) > $Na_v2.1$ (10.7%) > $Na_v1.3$ (4.6%) > $Na_v1.6$ (0.5%). It is, in part, in line with the results of previous studies. In rodents, $Na_v1.1$, $Na_v1.3$ and $Na_v1.6$ were initially found in the T tubules (Maier *et al.* 2002). In dog VCMs and Purkinje fibres, $Na_v1.1$ and both $Na_v1.2$ and $Na_v1.6$ were localized in the intercalated discs and at Z-lines, respectively (Haufe *et al.* 2005*a*,*b*). Therefore these studies suggest species-specific expression and protein localization within compartments of the sarcolemma. Immunoblot data exclude a membrane location for $Na_v1.3$, despite an abundant amount of mRNA in dog heart (Haufe *et al.* 2005*b*). We found expression of $Na_v2.1$ that has been previously discovered in uterus and human hearts ($hNa_v2.1$) and may represent a secondary Na_v subfamily (George *et al.* 1992; Felipe *et al.* 1994). Its function as a voltage-gated Na^+ channel has not been confirmed; therefore it is not likely to be a candidate for the I_{NaL} (Trimmer & Agnew, 1989; Watanabe *et al.* 2000). Further analysis of expression of other genes as possible candidates for I_{NaL} revealed HF-related

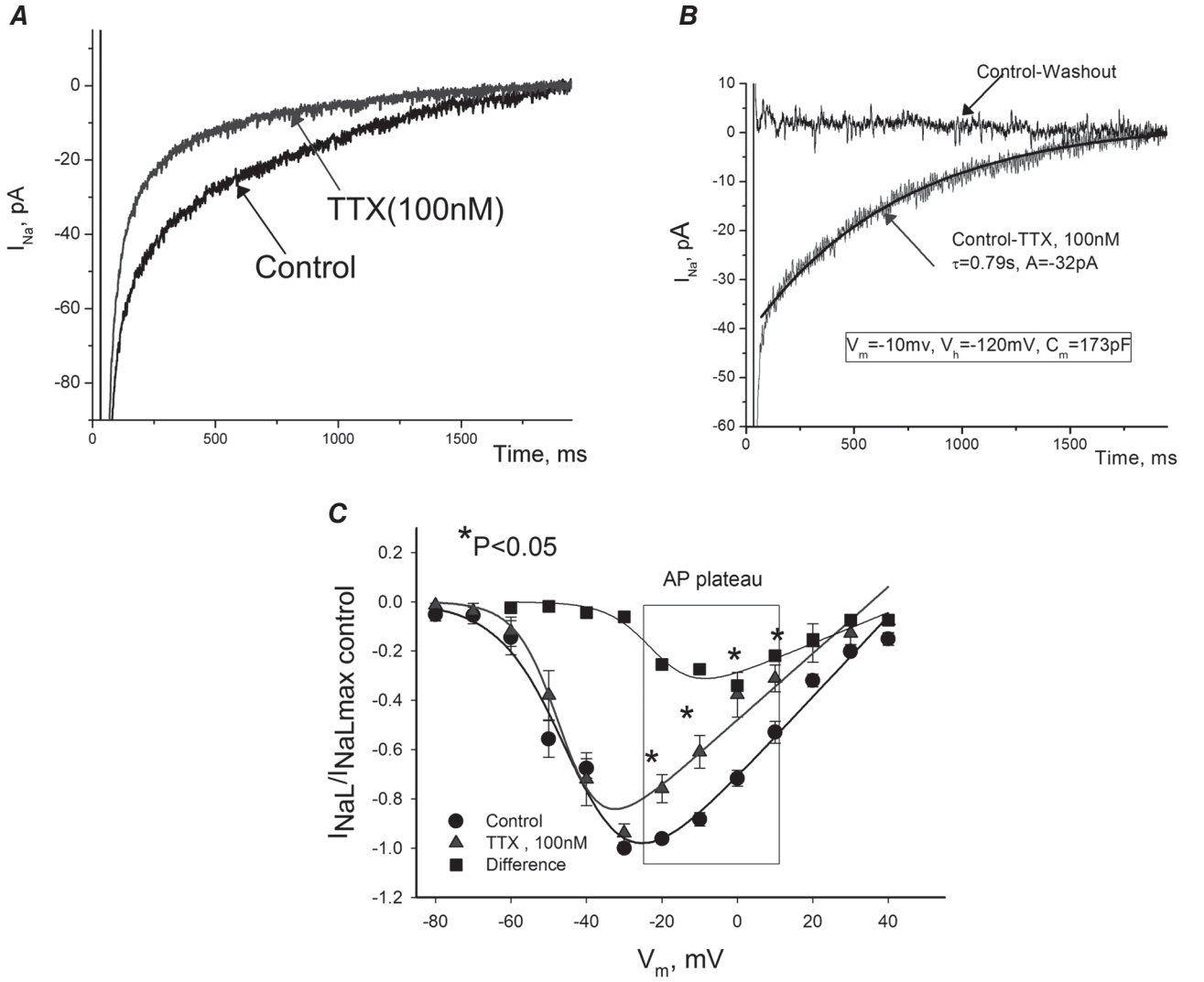

Figure 6. Contribution of tetrodotoxin (TTX)-sensitive neuronal Na_vs to I_{NaL} in failing dog ventricular cardiomyocytes
A, raw current traces recorded in cultured cells in which *SCN5A* was silenced by the virally delivered $Na_v1.5$-siRNA before and after TTX (100 nM). *B*, difference current (Control-TTX), or neuronal I_{NaL} component along with the best single-exponent fit. Zero current represents difference between control recording and after TTX washout. Fit parameters and voltage-clamp protocol (same for *A*) is given in the panel. *C*, normalized *I–V* relationship of I_{NaL} before and after TTX recorded in freshly isolated cells. Current density was evaluated as an average within 200–220 ms after depolarization pulse for 2 s, $V_h = -120$ mV. Continuous lines are theoretical curves of steady-state activation. Note that TTX produced SSA shift to left ($V_{1/2} = -43$ mV in control *vs.* –45 mV with TTX). Data are mean ± SEM.

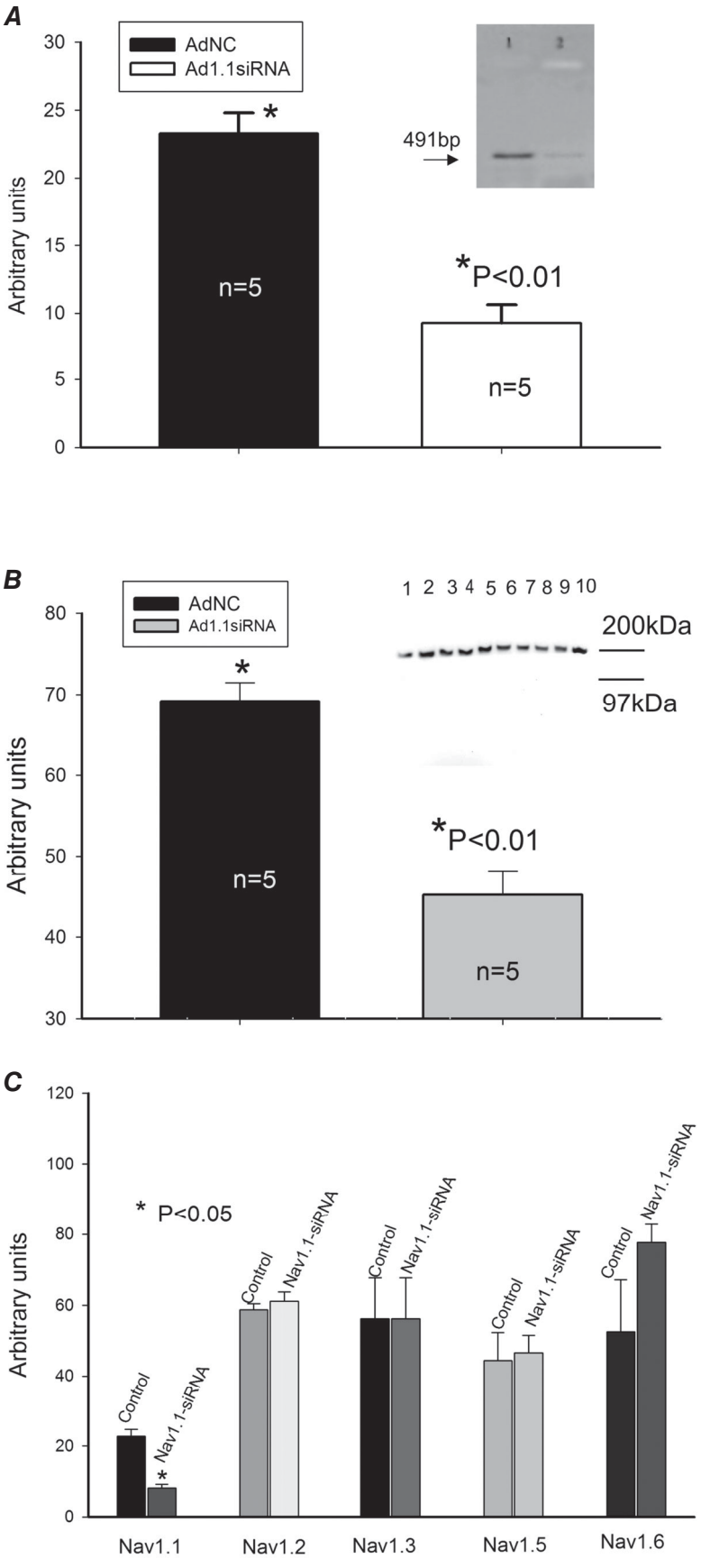

Figure 7. Silencing of *SCN1A* gene that encodes $Na_v1.1$ with adenovirus containing coding sequences for siRNA in cardiomyocytes from dogs with chronic HF
A, summary data of RT-PCR analysis of mRNA abundance (representative gels are shown in the inset at the upper right corner of the panel) in cultured dog cardiomyocytes. AdNC, adenovirus expressing non-specific siRNA as a control, Ad1.1siRNA, adenoviral construct expressing $Na_v1.1$ silencing sequences. *B*, summary data of Western blot analysis of $Na_v1.1$ protein abundance in cells treated with control virus (lanes 2–5 and 10 in the representative gels shown in the inset at the right upper corner of the panel) or $Na_v1.1$-siRNA (lanes 1 and 6–9, see inset). *C*, summary data of RT-PCR analysis of different Na^+ channel isoforms after transfection with $Na_v1.1$-siRNA (from 4 to 8 samples). *Statistically significant changes in *A*, *B* and *C* were evaluated by the ANOVA test followed by Bonferroni's *post hoc* test. Data are mean ± SEM.

changes in the expression of $Na_v1.1$ (up-regulation) and $Na_v1.6$ (down-regulation): at the same time no significant changes in transcripts of other Na^+ channel isoforms were detected. Therefore our focus was on $Na_v1.1$ as a plausible contributor to I_{NaL}. Our dog model is an ischaemic model of heart failure. We show that increased expression of $Na_v1.1$ in failing VCMs from dogs correlates with human ischaemic HF (IHF) (Fig. 1*A*). At the same time we did not find increased $Na_v1.1$ expression in ventricle tissue samples from human hearts with non-ischaemic HF.

The contributions of these isoforms to I_{NaL} under normal conditions and the changes of these contributions in different pathological conditions remain unknown. The molecular identity of I_{NaL} needs careful consideration especially for failing hearts where the gene expression profile changes dramatically. Using antisense inhibition by oligonucleotides, we have previously demonstrated that $Na_v1.5$ is a major contributor to I_{NaL} in normal dog heart (Maltsev *et al.* 2008*a*) and this finding was confirmed in the present study. At least 70% of I_{NaT} and I_{NaL} are related to this cardiac Na^+ channel isoform (see

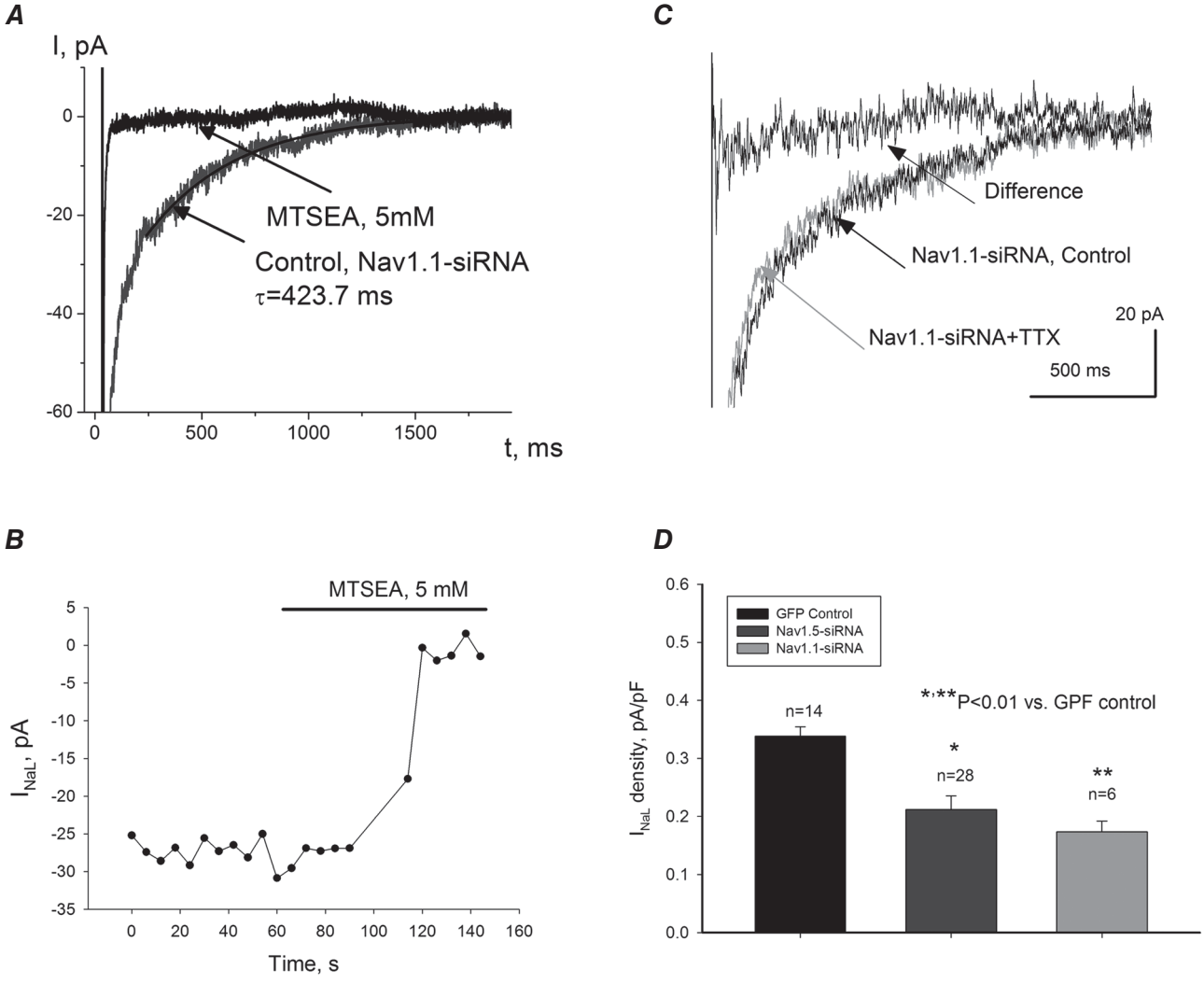

Figure 8. Contribution of neuronal $Na_v1.1$ to I_{NaL} in failing dog ventricular cardiomyocytes
In these cells expression of $Na_v1.1$ was silenced by virally delivered $Na_v1.1$-siRNA. *A*, raw current traces recorded before ($Na_v1.1$-siRNA, control) and after MTSEA application. Continuous line represents single exponent fit to I_{NaL} decay, and value of time constant, τ, is given at the trace. *B*, time course of I_{NaL} amplitude, evaluated between 200 and 220 ms after depolarization onset, during MTSEA application. *C*, raw current traces recorded before ($Na_v1.1$-siRNA, control) and after 100 nM TTX application ($Na_v1.1$-siRNA + TTX). The difference current was obtained by subtracting currents before and after TTX. *D*, summary data and statistical analysis of I_{NaL} current densities obtained in cells infected with virus that contains cDNA for GFP (GFP Control) for $Na_v1.5$-siRNA + GFP ($Na_v1.5$-siRNA) and for $Na_v1.1$-siRNA + GFP ($Na_v1.1$-siRNA). Current densities were measured 200 ms after depolarization to –10 mV onset. Statistical significance, $P < 0.01$, between experimental data points presented as mean ± SEM were evaluated by ANOVA followed by Bonferroni's *post hoc* test.

Figs 3–6). The late Na^+ channel openings are expected for at least $Na_v1.6$ (Welch *et al.* 2008) and have been reported also for $Na_v1.1$ (Aman *et al.* 2009). Therefore, the hypothesis of possible roles of the neuronal isoforms of Na^+ channel in Na^+-related Ca^{2+} signals in HF makes sense based on these previous data and is supported, in part, by our findings reported here. A contribution of $Na_v1.6$ to the mechanism of augmented I_{NaL} in HF is unlikely because it is down-regulated as we have discussed above. A separate study focusing on $Na_v1.6$ is required to understand its changes in failing hearts. The $Na_v1.1$ has been widely studied because of its involvement in the genetic epilepsy syndrome (Catterall *et al.* 2010). Not only mutant but also wild-type (to a lesser extent though) forms of these channels exhibit slow inactivation and persistent I_{Na}, which can be modulated by auxiliary β-subunits (Spampanato *et al.* 2004) similar to what we reported for $Na_v1.5$ (Maltsev *et al.* 2009; Mishra *et al.* 2011).

We demonstrated that β_1 and β_2 subunits act in opposite directions by enhancing or reducing I_{NaL} in normal and failing dog hearts. It is interesting to note that, similar to $Na_v1.5$ (Undrovinas *et al.* 2002; Maltsev & Undrovinas, 2006), the $Na_v1.1$ also demonstrates modal gating behaviour and can enter a slow mode that generates late openings (Vanoye *et al.* 2006). This modal shift can be enhanced or attenuated by β-auxiliary subunits (Spampanato *et al.* 2004).

Physiological importance of neuronal Na_vs in heart

The neuronal component of I_{NaL} is a significant contributor to AP duration and shape because of its biophysical properties such as a relatively high level of midpoint for steady-state activation and inactivation and a relatively slow decay time course (*vs.* cardiac type I_{NaL}). Our numerical model simulations demonstrated

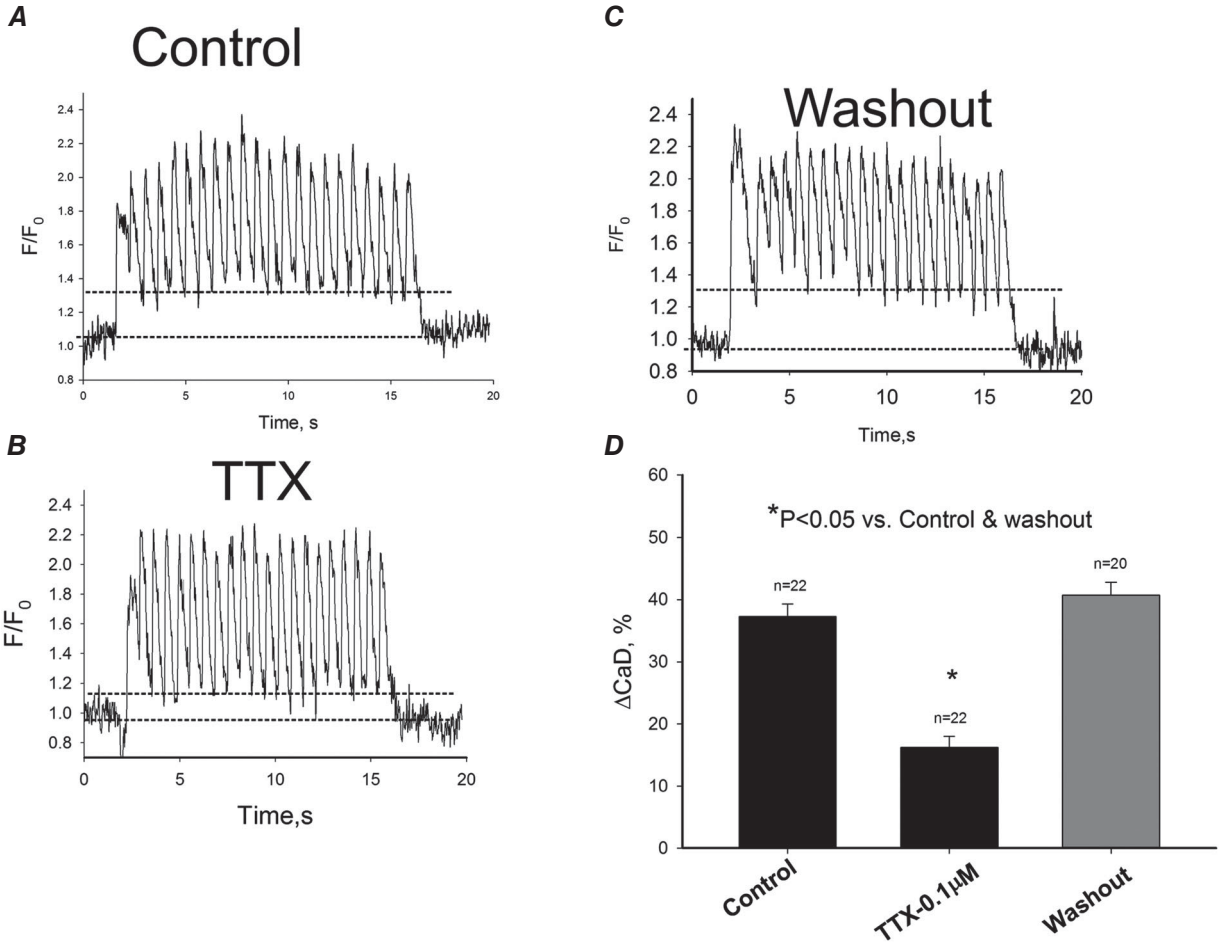

Figure 9. Blockade of neuronal Na^+ channels by 100 nm TTX reversibly attenuates diastolic intracellular Ca^{2+} elevation in ventricular cardiomyocytes of dogs with chronic heart failure
Intracellular Ca^{2+} dynamics recorded during 1.5 Hz pulse train in control (*A*), in the presence of 100 nM TTX (*B*) and after the toxin washout (*C*). Dotted lines in *A*, *B* and *C* refer to average diastolic Ca^{2+} levels before and during pulse train. *D*, data summary for diastolic Ca^{2+} (CaD) changes (ΔCaD) in response to the pulse train. Data are mean ± SEM, cell numbers are given above the bars. $^*P < 0.05$, ANOVA followed by Bonferroni's *post hoc* test.

that, despite a smaller initial density of the neuronal component (after membrane depolarization) *vs.* cardiac I_{NaL}, its ratio to the cardiac I_{NaL} increases during AP plateau and becomes comparable to the cardiac component at the end of the AP plateau (see Fig. 10*B*). Therefore targeting the neuronal component of I_{NaL} can be an effective strategy to reduce AP duration and its variability in HF (Fig. 10*C*). We demonstrate that blockade of the neuronal I_{NaL} component by a low TTX concentration reduces diastolic Ca^{2+} accumulation in both experiments (Fig. 9) and *in silico* simulations (Fig. 10*D*). Therefore this neuronal I_{NaL} component is probably involved in abnormalities of E–C coupling in failing heart, such as diastolic dysfunction, i.e. the reduced ability of the myocardium to relax during diastole. In contrast, TTX-sensitive I_{Na} was not implicated in triggered Ca^{2+} release from sarcoplasmic reticulum (SR) in rodent VCMs and the authors claimed no apparent commitment for neuronal Na_vs in E–C coupling (Brette &

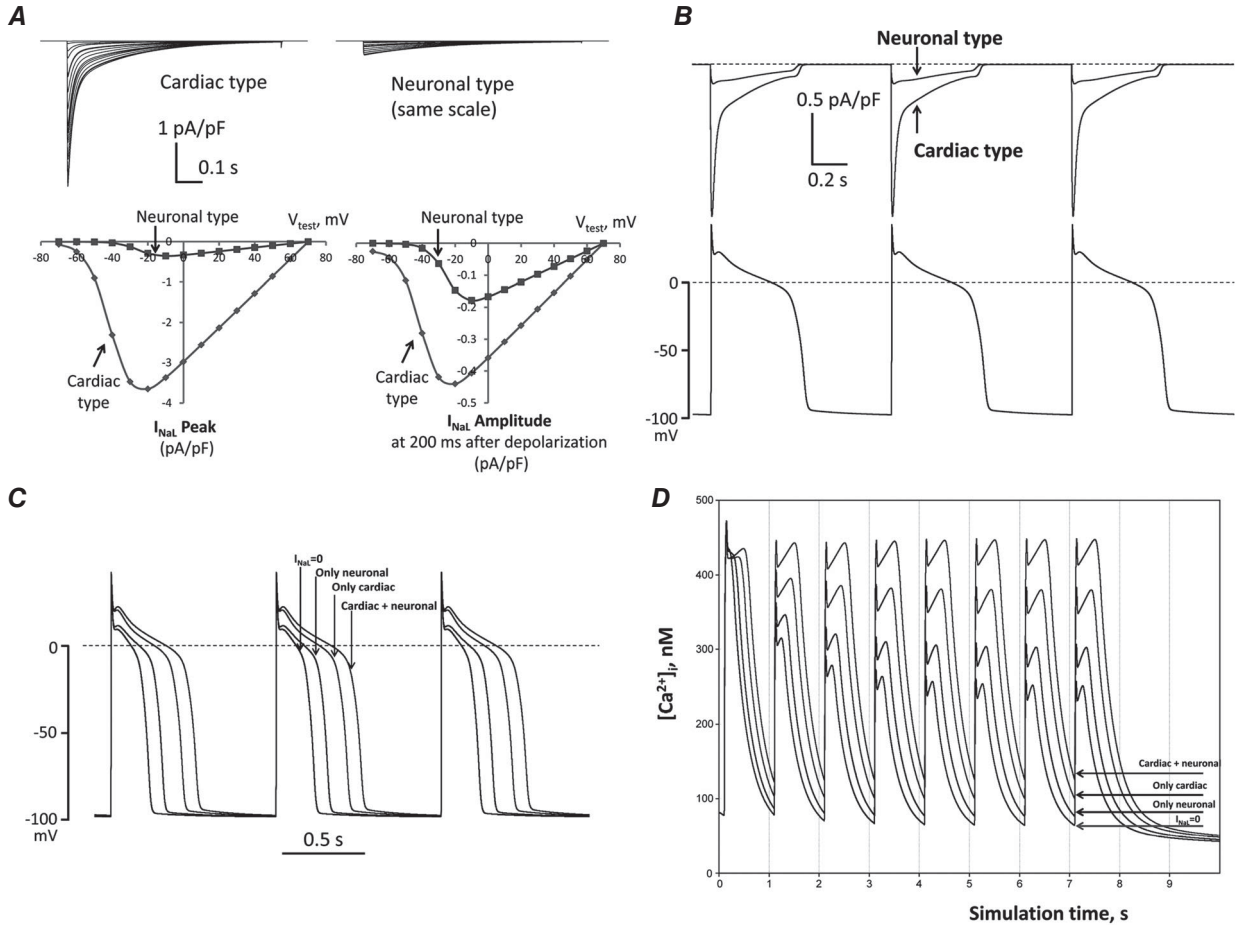

Figure 10. *In silico* investigation on neuronal and cardiac I_{NaL} components in HF dog ventricular cell
A, predicted current–voltage relationships. The upper panels show families of predicted current traces at different membrane voltages for the cardiac and neuronal Na_v components. The lower panels show plotted amplitude values of these predictions. Left lower sub-panel shows the peak I_{NaL} (at zero time after the depolarization onset) and right lower sub-panel shows the current amplitudes 200 ms after depolarization onset. Holding potential was $V_h = -120$ mV, test pulses were applied from –70 mV to +70 mV. *B*, predicted profile of I_{NaL} generated by cardiac and neuronal Na_vs in numerical model simulations of AP. *C* and *D*, predicted differential contribution of I_{NaL} by the neuronal and cardiac Na_vs to shape and duration of AP and intracellular Ca^{2+} dynamics, respectively, at the pacing rate of 1 Hz. Complete I_{NaL} elimination from simulations ($I_{NaL} = 0$) reduces AP duration and eliminates diastolic Ca^{2+} accumulation. Introduction of only the cardiac or neuronal component of I_{NaL} increases AP duration and leads to diastolic Ca^{2+} accumulation, whereas incorporation of both I_{NaL} components, which reflects the situation *in situ,* affects these physiological responses dramatically. All numerical simulations were performed at a physiological temperature of 37 °C using our modification of the Winslow E–C coupling model of canine failing VCMs (Winslow *et al.* 1999) with formulations for I_{NaL} which were previously developed based on our experimental voltage-clamp data (Undrovinas *et al.* 2010; Mishra *et al.* 2011). In the present study I_{NaL} formulations included two separate I_{NaL} components for cardiac and neuronal isoforms, respectively. Each component has its own activation and inactivation gating variables evaluated from patch-clamp data obtained in the present study (see section 'Patch-clamp data').

Orchard, 2006). This discrepancy can be explained in two ways: (1) E–C coupling in rodents *versus* large animals, such as dog, as well as in humans, is different in the way that the source of Ca^{2+} involved in contraction is mainly stored in SR and is less (or almost not) dependent on transmembrane ion fluxes during AP development, and (2) in rodents, heart rate is very high and APs are very short, therefore I_{NaL} does not play the same role as in humans or dogs. Since late openings of Na^+ channels generate both electric current and Na^+ influx during the AP plateau, I_{NaL} is expected to contribute to at least two known HF cellular mechanisms: (1) electrophysiological remodelling, and (2) altered cell Na^+ cycling. The latter mechanism is tightly integrated with Ca^{2+} cycling, as Na^+ modulates the Na^+–Ca^{2+} exchanger operation (Bers *et al.* 2006). Therefore the neuronal component of I_{NaL} can also play a role in the impaired E–C coupling in HF via Na^+ balance and its interplay with Ca^{2+} handling and signalling. Haufe *et al.* (2005*b*) suggested that neuronal Na_vs might act as a safety mechanism. Because of the biophysical properties of neuronal Na_vs (SSI and SSA are shifted to more depolarized potentials compared to that for $Na_v1.5$) this safety mechanism can be recruited under pathological conditions, when the resting membrane potential is depolarized.

Study limitations

The relative mRNA abundance expressed as arbitrary units was calculated using the expression levels of all transcripts normalized to GAPDH mRNA. There are some indications that GAPDH expression can change in atria *vs.* ventricles in patients with HF. Since in this study we did not compare atria *vs.* ventricles in humans we assume that GAPDH can serve as a valid marker. According to previous studies by our group and others, levels of mRNA for this marker gene do not change in the left ventricle dog or mini pig HF model (Mishra *et al.* 2005; Imai *et al.* 2007; Martino *et al.* 2011). Therefore we are confident that our data are not affected because of this marker choice.

The human data are based on ventricular tissue mRNA analysis, rather than isolated myocytes. It could be, in part, contaminated with mRNA from neurons that can be found in ventricles. We found a very similar pattern of Na_v expression in these samples when compared with samples from isolated myocytes of dog. Therefore we believe that our conclusions are valid.

New strategy to treat HF-related deficiencies

The paradigm in HF for the Na^+ current is that I_{NaT}, responsible for the AP upstroke and propagation, is down-regulated, whereas I_{NaL} is up-regulated and involved in repolarization and Ca^{2+}-handling abnormalities. A direct blockade of Na^+ channels by Class I drugs is not acceptable as a therapeutic strategy in HF, because it leads to further reduction in propagation velocity and increases the probability of excitation propagation blockade or re-entrant arrhythmias. The discovery of a new neuronal component of I_{NaL} allows a new differential treatment of rhythm abnormalities and contractility deficiency as discussed above. The treatment can include a specific neuronal channel blocker or genetic approaches to specifically reduce the neuronal I_{NaL} component in heart that is especially important for the late AP plateau phase (Fig. 10*C*) (due to its relatively slow decay, see Fig. 6*A*) but is probably less important for cell excitability (due to its relatively higher activation voltage).

In conclusion we have discovered an *SCN1A*-related $Na_v1.1$ component of I_{NaL} in ventricular myocytes of dog with heart failure. This component is physiologically relevant to controlling AP shape and duration as well as Ca^{2+} dynamics.

References

Aman TK, Grieco-Calub TM, Chen C, Rusconi R, Slat EA, Isom LL & Raman IM (2009). Regulation of persistent Na current by interactions between β subunits of voltage-gated Na channels. *J Neurosci* **29**, 2027–2042.

Bers DM, Despa S & Bossuyt J (2006). Regulation of Ca^{2+} and Na^+ in normal and failing cardiac myocytes. *Ann N Y Acad Sci* **1080**, 165–177.

Brette F & Orchard CH (2006). No apparent requirement for neuronal sodium channels in excitation-contraction coupling in rat ventricular myocytes. *Circ Res* **98**, 667–674.

Catterall WA, Kalume F & Oakley JC (2010). $Na_V1.1$ channels and epilepsy. *J Physiol* **588**, 1849–1859.

Coraboeuf E, Deroubaix E & Coulombe A (1979). Effect of tetrodotoxin on action potentials of the conducting system in the dog heart. *Am J Physiol Heart Circ Physiol* **236**, H561–H567.

Elbashir SM, Lendeckel W & Tuschl T (2001). RNA interference is mediated by 21- and 22-nucleotide RNAs. *Genes Dev* **15**, 188–200.

Felipe A, Knittle TJ, Doyle KL & Tamkun MM (1994). Primary structure and differential expression during development and pregnancy of a novel voltage-gated sodium channel in the mouse. *J Biol Chem* **269**, 30125–30131.

George AL Jr, Knittle TJ & Tamkun MM (1992). Molecular cloning of an atypical voltage-gated sodium channel expressed in human heart and uterus: evidence for a distinct gene family. *Proc Natl Acad Sci U S A* **89**, 4893–4897.

Haufe V, Camacho JA, Dumaine R, Gunther B, Bollensdorff C, von Banchet GS, Benndorf K & Zimmer T (2005*a*). Expression pattern of neuronal and skeletal muscle voltage-gated Na^+ channels in the developing mouse heart. *J Physiol* **564**, 683–696.

Haufe V, Cordeiro JM, Zimmer T, Wu YS, Schiccitano S, Benndorf K & Dumaine R (2005*b*). Contribution of neuronal sodium channels to the cardiac fast sodium current I_{Na} is greater in dog heart Purkinje fibers than in ventricles. *Cardiovasc Res* **65**, 117–127.

Imai M, Rastogi S, Gupta RC, Mishra S, Sharov VG, Stanley WC, Mika Y, Rousso B, Burkhoff D, Ben-Haim S & Sabbah HN (2007). Therapy with cardiac contractility modulation electrical signals improves left ventricular function and remodeling in dogs with chronic heart failure. *J Am Coll Cardiol* **49**, 2120–2128.

Logeart D, Gueffet JP, Rouzet F, Pousset F, Chavelas C, Solal AC & Jondeau G (2009). Heart rate per se impacts cardiac function in patients with systolic heart failure and pacing: a pilot study. *Eur J Heart Fail* **11**, 53–57.

Maier SK, Westenbroek RE, McCormick KA, Curtis R, Scheuer T & Catterall WA (2004). Distinct subcellular localization of different sodium channel α and β subunits in single ventricular myocytes from mouse heart. *Circulation* **109**, 1421–1427.

Maier SK, Westenbroek RE, Schenkman KA, Feigl EO, Scheuer T & Catterall WA (2002). An unexpected role for brain-type sodium channels in coupling of cell surface depolarization to contraction in the heart. *Proc Natl Acad Sci U S A* **99**, 4073–4078.

Maltsev VA, Kyle JW, Mishra S & Undrovinas A (2008*a*). Molecular identity of the late sodium current in adult dog cardiomyocytes identified by $Na_v1.5$-antisense inhibition. *Am J Physiol Heart Circ Physiol* **295**, H667–H676.

Maltsev VA, Kyle JW & Undrovinas A (2009). Late Na^+ current produced by human cardiac Na^+ channel isoform $Na_v1.5$ is modulated by its β_1 subunit. *J Physiol Sci* **59**, 217–225.

Maltsev VA, Reznikov V, Undrovinas NA, Sabbah HN & Undrovinas A (2008*b*). Modulation of the late sodium current by Ca^{2+}, calmodulin, and CaMKII in normal and failing dog cardiomyocytes: similarities and differences. *Am J Physiol Heart Circ Physiol* **294**, H1597–H1608.

Maltsev VA, Sabbah HN, Higgins RSD, Silverman N, Lesch M & Undrovinas AI (1998*a*). Novel, ultraslow inactivating sodium current in human ventricular cardiomyocytes. *Circulation* **98**, 2545–2552.

Maltsev VA, Sabbah HN, Tanimura M, Lesch M, Goldstein S & Undrovinas AI (1998*b*). Relationship between action potential, contraction-relaxation pattern, and intracellular Ca^{2+} transient in cardiomyocytes of dogs with chronic heart failure. *Cell Mol Life Sci* **54**, 597–605.

Maltsev VA, Sabbah HN & Undrovinas AI (2001). Late sodium current is a novel target for amiodarone: Studies in failing human myocardium. *J Mol Cell Cardiol* **33**, 923–932.

Maltsev VA, Sabbah HN & Undrovinas AI (2002). Down-regulation of sodium current in chronic heart failure: effects of long-term therapy with carvedilol. *Cell Mol Life Sci* **59**, 1561–1568.

Maltsev VA, Silverman N, Sabbah HN & Undrovinas AI (2007). Chronic heart failure slows late sodium current in human and canine ventricular myocytes: Implications for repolarization variability. *Eur J Heart Fail* **9**, 219–227.

Maltsev VA & Undrovinas A (2008). Late sodium current in failing heart: Friend or foe? *Prog Biophys Mol Biol* **96**, 421–451.

Maltsev VA & Undrovinas AI (1997). Cytoskeleton modulates coupling between availability and activation of cardiac sodium channel. *Am J Physiol Heart Circ Physiol* **273**, H1832–H1840.

Maltsev VA & Undrovinas AI (2006). A multi-modal composition of the late Na^+ current in human ventricular cardiomyocytes. *Cardiovasc Res* **69**, 116–127.

Martino A, Cabiati M, Campan M, Prescimone T, Minocci D, Caselli C, Rossi AM, Giannessi D & Del Ry S (2011). Selection of reference genes for normalization of real-time PCR data in minipig heart failure model and evaluation of TNF- α mRNA expression. *J Biotechnol* **153**, 92–99.

Mishra S, Sabbah HN, Rastogi S, Imai M & Gupta RC (2005). Reduced sarcoplasmic reticulum Ca^{2+} uptake and increased Na^+-Ca^{2+} exchanger expression in left ventricle myocardium of dogs with progression of heart failure. *Heart Vessels* **20**, 23–32.

Mishra S, Undrovinas NA, Maltsev VA, Reznikov V, Sabbah HN & Undrovinas A (2011). Post-transcriptional silencing of SCN1B and SCN2B genes modulates late sodium current in cardiac myocytes from normal dogs and dogs with chronic heart failure. *Am J Physiol Heart Circ Physiol* **301**, H1596–H1605.

Noble D & Noble PJ (2006). Late sodium current in the pathophysiology of cardiovascular disease: consequences of sodium-calcium overload. *Heart* **92**, Suppl. 4, iv1–iv5.

Rao K, Fisher ML, Robinson S, Shorofsky S & Gottlieb SS (2007). Effect of chronic changes in heart rate on congestive heart failure. *J Card Fail* **13**, 269–274.

Sabbah HN, Goldberg AD, Schoels W, Kono T, Webb C, Brachmann J & Goldstein S (1992). Spontaneous and inducible ventricular arrhythmias in a canine model of chronic heart failure: relation to haemodynamics and sympathoadrenergic activation. *Eur Heart J* **13**, 1562–1572.

Sabbah HN, Stein PD, Kono T, Gheorghiade M, Levine TB, Jafri S, Hawkins ET & Goldstein S (1991). A canine model of chronic heart failure produced by multiple sequential coronary microembolizations. *Am J Physiol Heart Circ Physiol* **260**, H1379–H1384.

Spampanato J, Kearney JA, de Haan G, McEwen DP, Escayg A, Aradi I, MacDonald BT, Levin SI, Soltesz I, Benna P, Montalenti E, Isom LL, Goldin AL & Meisler MH (2004). A novel epilepsy mutation in the sodium channel *SCN1A* identifies a cytoplasmic domain for β subunit interaction. *J Neurosci* **24**, 10022–10034.

Trimmer JS & Agnew WS (1989). Molecular diversity of voltage-sensitive Na channels. *Annu Rev Physiol* **51**, 401–418.

Undrovinas AI, Belardinelli L, Undrovinas NA & Sabbah HN (2006). Ranolazine improves abnormal repolarization and contraction in left ventricular myocytes of dogs with heart failure by inhibiting late sodium current. *J Cardiovasc Electrophysiol* **17**, S169–S177.

Undrovinas AI, Fleidervish IA & Makielski JC (1992). Inward sodium current at resting potentials in single cardiac myocytes induced by the ischemic metabolite lysophosphatidylcholine. *Circ Res* **71**, 1231–1241.

Undrovinas A & Maltsev VA (2008). Late sodium current is a new therapeutic target to improve contractility and rhythm in failing heart. *Cardiovasc Hematol Agents Med Chem* **6**, 348–359.

Undrovinas NA, Maltsev VA, Belardinelli L, Sabbah HN & Undrovinas A (2010). Late sodium current contributes to diastolic cell Ca^{2+} accumulation in chronic heart failure. *J Physiol Sci* **60**, 245–257.

Undrovinas AI, Maltsev VA, Kyle JW, Silverman NA & Sabbah HN (2002). Gating of the late Na^+ channel in normal and failing human myocardium. *J Mol Cell Cardiol* **34**, 1477–1489.

Undrovinas AI, Maltsev VA & Sabbah HN (1999). Repolarization abnormalities in cardiomyocytes of dogs with chronic heart failure: Role of sustained inward current. *Cell Mol Life Sci* **55**, 494–505.

Undrovinas AI, Shander GS & Makielski JC (1995). Cytoskeleton modulates gating of voltage-dependent sodium channel in heart. *Am J Physiol Heart Circ Physiol* **269**, H203–H214.

Valdivia CR, Chu WW, Pu J, Foell JD, Haworth RA, Wolff MR, Kamp TJ & Makielski JC (2005). Increased late sodium current in myocytes from a canine heart failure model and from failing human heart. *J Mol Cell Cardiol* **38**, 475–483.

Vanoye CG, Lossin C, Rhodes TH & George AL Jr (2006). Single-channel properties of human $Na_V1.1$ and mechanism of channel dysfunction in *SCN1A*-associated epilepsy. *J Gen Physiol* **127**, 1–14.

Watanabe E, Fujikawa A, Matsunaga H, Yasoshima Y, Sako N, Yamamoto T, Saegusa C & Noda M (2000). Na_v2/NaG channel is involved in control of salt-intake behavior in the CNS. *J Neurosci* **20**, 7743–7751.

Welch NC, Lin W, Juranka PF, Morris CE & Stys PK (2008). Traditional AMPA receptor antagonists partially block $Na_v1.6$-mediated persistent current. *Neuropharmacology* **55**, 1165–1171.

Winslow RL, Rice J, Jafri S, Marbán E & O'Rourke B (1999). Mechanisms of altered excitation-contraction coupling in canine tachycardia-induced heart failure, II: model studies. *Circ Res* **84**, 571–586.

Zicha S, Maltsev VA, Nattel S, Sabbah HN & Undrovinas AI (2004). Post-transcriptional alterations in the expression of cardiac Na^+ channel subunits in chronic heart failure. *J Mol Cell Cardiol* **37**, 91–100.

Additional information

Competing interests

The authors have no competing interests to declare.

Author contributions

Conception, analysis and design of the experiments: A.U. Collection, analysis and interpretation of data: S.M., V.R., V.A.M., N.A.U. and A.U. Dog chronic heart failure model and mathematical modelling: H.N.S. and V.A.M. Drafting the article or reviewing it critically for important intellectual content: A.U., V.A.M., H.N.S. and S.M. All authors approved the final version of the manuscript.

Funding

This study was supported by National Heart, Lung, and Blood Institute Grants HL-53819 and HL-074238, by a grant-in-aid from the American Heart Association (0350472Z; to A. Undrovinas), and, in part, by the Intramural Research Program of the National Institute on Aging (to V. A. Maltsev; the numerical modelling part).

Author's present address

S. Mishra: Department of Translational Science and Molecular Medicine, MSU College of Human Medicine, Grand Rapids, MI, USA.